

High-Sensitivity Quantum-Enhanced Interferometers

Juan Yu ^{1,*} , Yinhua Wu ¹, Liang Nie ¹ and Xiaojie Zuo ²¹ School of Optoelectronic Engineering, Xi'an Technological University, Xi'an 710021, China² School of Electronic and Intelligentization, Dongguan University of Technology, Dongguan 523808, China

* Correspondence: yuj@xatu.edu.cn

Abstract: High-sensitivity interferometers are one of the basic tools for precision measurement, and their sensitivity is limited by their shot noise limit (SNL), which is determined by vacuum fluctuations of the probe field. The quantum interferometer with novel structures can break the SNL and measure the weak signals, such as the direct observation of gravity wave signal. Combining classical interferometers and the optical parametric amplifier (OPA) can enhance the signal; meanwhile, the quantum noise is kept at the vacuum level, so that the sensitivity of the nonlinear interferometer beyond the SNL can be achieved. By analyzing in detail the influence of system parameters on the precision of quantum metrology, including the intensity of optical fields for phase sensing, the gain factor of OPA, and the losses inside and outside the interferometers, the application conditions of high-sensitivity nonlinear quantum interferometers are obtained. Quantum interferometer-based OPAs provide the direct references for the practical development of quantum precise measurement.

Keywords: quantum metrology; interferometer; optical parametric amplifier; shot noise limit

1. Introduction

Metrology underpins quantitative science, and the improvement of measurement precision leads not only to extensive detailed knowledge, but also to a new fundamental understanding of nature. The optical interferometer is one of the most powerful metrology tools, and the phase change of light in the interferometer is quite sensitive to a variety of variances of physical quantities influencing the optical path, such as biological samples [1] continuous force, and displacement [2]. Interferometers play a key role in precision measurements for gravitational waves [3–5], gravity fields [6,7], imaging [8], and so on. The measurement precision for a classical optical device is limited by the shot noise limit (SNL): $\delta_{\text{SNL}} = 1/\sqrt{N}$ [9] (where N is the photon number of the phase-sensitive field), because of the vacuum fluctuation of quantized electromagnetic field. The ultimate limit of sensitivity is named as the Heisenberg limit (HL): $\delta_{\text{HL}} = 1/N$ [10], which is given by Heisenberg uncertainty in quantum mechanics. Quantum resources can be employed to improve the measurement precision to break through the classical limit SNL [11,12] and approach the quantum limit HL [13–15].

Since a quantum state is proposed to break the limit of shot noise in 1981 [16], many optical systems [17–23] have proved that quantum states, such as squeezed state and entangled states, can greatly improve the measurement precision at a given photon number [24]. On the other hand, interferometers with novel structures can provide an alternative way to achieve high-precision phase estimation [25]. The optical parametric amplifier (OPA) is a stable solid quantum device to be applied for realizing metrology, because of both favorable features of shot noise squeezing and signal amplification [26–30]. Parametric processing has been widely adopted in the construction of quantum interferometers [31–35] and several groups have also demonstrated the quantum-enhanced measurement of microscopic cantilever displacement based on utilizing truncated SU(1,1) interferometers [36]. Very recently, significant progress has been made with quantum interferometers [37–40].



Citation: Yu, J.; Wu, Y.; Nie, L.; Zuo, X. High-Sensitivity Quantum-Enhanced Interferometers. *Photonics* **2023**, *10*, 749. <https://doi.org/10.3390/photonics10070749>

Received: 7 June 2023

Revised: 22 June 2023

Accepted: 26 June 2023

Published: 29 June 2023



Copyright: © 2023 by the authors. Licensee MDPI, Basel, Switzerland. This article is an open access article distributed under the terms and conditions of the Creative Commons Attribution (CC BY) license (<https://creativecommons.org/licenses/by/4.0/>).

In this study, we investigate two kinds of quantum-interferometer-based parametric amplification. On one hand, a quantum Michelson interferometer (QMI) consisting of OPA, which is a nonlinear element to split and recombine the signal field, can enhance the signal, and the quantum noise is kept at the vacuum level, so that the sensitivity beyond the SNL is achieved. On the other hand, a quantum Mach–Zehnder interferometer (QMZI) can be constructed by placing two OPAs placed in two arms of the interferometer, respectively. The squeezed state generated by the OPAs within the QMZI was directly used as a phase-sensitive quantum state. In realistic situations, the measurement system is rarely isolated and is inevitably affected by the environment. The losses are one of the main obstacles to the realization of quantum measurement [30]. We compare and analyze the relationship between measurement sensitivity and system parameters of the two kinds of quantum interferometers, including the intensity of optical fields for phase sensing, the gain factor of OPA, and the losses inside and outside the interferometers. The quantum interferometer not only squeezes shot noise but also amplifies the phase-sensing intensity to realize the sensitivity beyond the SNL. Through analyzing in detail the influence of system parameters on the precision of quantum metrology, the experimental parameters for the further optimization of the performance of high-sensitivity nonlinear quantum interferometers are obtained. Our result provides direct reference for the practical development of high precision quantum metrology.

2. Quantum Interferometers

An optical field can be represented by the annihilation operator \hat{a} in quantum mechanics. The orthogonal amplitude and phase operators can be represented in terms of the creation and annihilation operators, as $\hat{x} = (\hat{a} + \hat{a}^\dagger)$ and $\hat{p} = i(\hat{a}^\dagger - \hat{a})$, \hat{x} and \hat{p} satisfy the commutation relations $[\hat{x}, \hat{p}] = i$. Usually, a coherent state or a vacuum state is a minimum uncertainty state, and the variances of the two quadrature components are equal: $\langle \Delta^2 \hat{x} \rangle = \langle \Delta^2 \hat{p} \rangle = 1$. The linear Michelson interferometer (LMI) and QMI based on OPA are shown in Figure 1a,b. A 50:50 beam splitter (BS) is used for wave splitting and wave recombination, and the two arms of the interferometer are equal in optical path and perpendicular to each other in LMI. The two polarization beam splitters (PBS1 and PBS2) and the nondegenerate optical parametric amplifier (OPA) are equivalent to the 50:50 BS of LMI to realize the splitting and combining of optical fields, as shown in Figure 1b. The coherent state \hat{a}_{in} and the vacuum state \hat{b}_{in} are injected into the interferometer and split into two modes: \hat{A} and \hat{B} ; the two modes \hat{A} and \hat{B} return through the high-reflection mirrors in the two arms to be \hat{C} and \hat{D} , respectively. A phase shift ϕ is introduced on mode \hat{D} , and the amplified phase signal can be obtained by detecting the output optical field \hat{b}_{out} of the interferometer.

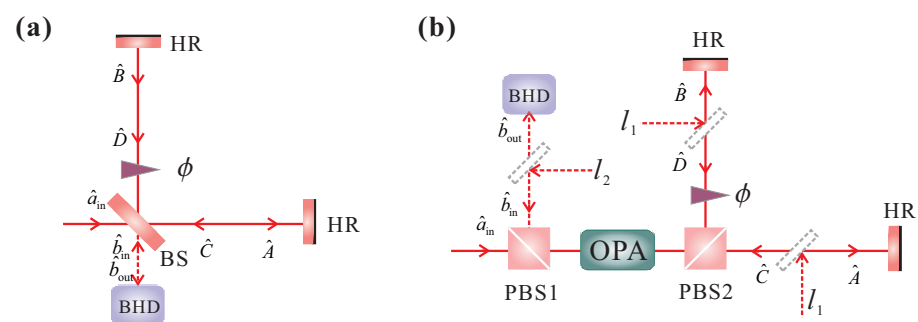


Figure 1. (a,b) Schematic diagrams of linear Michelson interferometer and quantum Michelson interferometer based on OPA, respectively. The coherent state \hat{a}_{in} and the vacuum state \hat{b}_{in} are injected into the interferometer and the phase signal can be obtained by detecting the output optical field \hat{b}_{out} . OPA, optical parametric amplifier; BHD, balanced homodyne detection; BS, 50:50 beam splitter; HR, high-reflection mirror; PBS_{1,2}, polarization beam splitter; ϕ , phase shift; l_1 , internal loss of single arm; l_2 , total external loss.

The input fields are amplified by OPA in interferometer [41]:

$$\begin{aligned} \hat{A} &= G\hat{a}_{in} + g\hat{b}_{in}^\dagger, \\ \hat{B} &= G\hat{b}_{in} + g\hat{a}_{in}^\dagger, \end{aligned} \tag{1}$$

where the amplifiers are assumed to be identical with G as the amplitude gain and $|G|^2 - |g|^2 = 1$. The optical fields \hat{C} and \hat{D} are described as follows:

$$\begin{aligned} \hat{C} &= \sqrt{1-l_1}(\sqrt{1-l_1}\hat{A} + \sqrt{l_1}\hat{A}_0) + \sqrt{l_1}\hat{C}_0, \\ \hat{D} &= \sqrt{1-l_1}(\sqrt{1-l_1}\hat{B}e^{i\phi} + \sqrt{l_1}\hat{B}_0) + \sqrt{l_1}\hat{D}_0, \end{aligned} \tag{2}$$

where l_1 is the single-arm transmission loss inside the interferometer; $\hat{A}_0, \hat{B}_0, \hat{C}_0, \hat{D}_0$ are the vacuum noises introduced by losses of the interferometer. The output field \hat{b}_{out} of the quantum interferometer is

$$\hat{b}_{out} = \sqrt{1-l_2}(G\hat{D} + g\hat{C}^\dagger) + \sqrt{l_2}\hat{E}_0, \tag{3}$$

where l_2 is the total loss outside the interferometer, which includes transmission loss, the interference efficiency of the quantum interferometer, and detection efficiency; \hat{E}_0 is the vacuum noise introduced by loss l_2 . The relative phase between the two arms of the interferometer is kept as $\phi = \pi + \delta$ ($\delta \ll 1$), where δ is the phase change, and it can be obtained by measuring the quadrature phase \hat{p} of the output field \hat{b}_{out} via balanced homodyne detection (BHD). The noise of the interferometric output field is

$$\langle \hat{p}_{b_{out}}^2 \rangle = 1 + 2g^2l_1(2-l_1)(1-l_2) + 4G^2(1-l_1)^2(1-l_2)I_{ps}^M\delta^2, \tag{4}$$

where the phase-sensing intensity is $I_{ps}^M = \langle \hat{D}^\dagger \hat{D} \rangle = g^2(1/2\alpha_{in}^2 + 1)$, α_{in}^2 is the input intensity of the interferometer. Then, the sensitivity of QMI can be obtained:

$$\delta_{QMI} = \sqrt{\frac{1 + 2g^2l_1(2-l_1)(1-l_2)}{4G^2(1-l_1)^2(1-l_2)I_{ps}^M}}, \tag{5}$$

Sensitivity of QMI is enhanced by a factor of $\sqrt{2G^2}$, comparing the sensitivity of LMI ($\delta_{LMI} = \sqrt{1/2I_{ps}}$, which is the corresponding SNL) in the lossless case.

The schematic diagrams of the linear Mach-Zehnder interferometer (LMZI) and QMZI based on OPAs are shown in Figure 2a,b. Two input fields (a coherent field \hat{a}_{in} and a vacuum state \hat{b}_{in}) and two 50:50 BSs are constructed a typical LMZI. Two OPAs are employed in two arms of QMZI to reduce the noise of the interferometer and amplify the phase-sensing intensity. The coherent state \hat{a}_{in} and the vacuum state \hat{b}_{in} are injected into the interferometer and split into two optical fields, \hat{A} and \hat{B} , by BS1. The beams \hat{A} and \hat{B} are amplified by two OPAs to be \hat{C} and \hat{D} , respectively. The mode \hat{D} undergoes a phase shift ϕ , and successively, the two beams are recombined by BS2 to produce the output field \hat{b}_{out} . The resultant output interference signal \hat{b}_{out} is sensitive to the phase change.

The input-output relations for the first linear 50:50 BS in interferometer are given by

$$\begin{aligned} \hat{A} &= (\hat{a}_{in} - \hat{b}_{in})/\sqrt{2}, \\ \hat{B} &= (\hat{a}_{in} + \hat{b}_{in})/\sqrt{2}, \end{aligned} \tag{6}$$

When the OPAs operate on the parametric amplification condition, the optical fields \hat{C} and \hat{D} can be described as follows:

$$\begin{aligned} \hat{C} &= G\hat{A} + g\hat{A}^\dagger, \\ \hat{D} &= G\hat{B} + g\hat{B}^\dagger, \end{aligned} \tag{7}$$

The relative phase between the two arms of the interferometer is kept to be $\phi = \pi + \delta$ ($\delta \ll 1$), and then, we find that the noise of interferometric output field is

$$\langle \hat{p}_{\hat{b}_{out}}^2 \rangle = 1 + (1 - l_1)(1 - l_2)[(G - g)^2 - 1] + 2(1 - l_1)(1 - l_2)(I_{ps}^{MZ} - g^2)\delta^2, \quad (8)$$

where the phase-sensing intensity is $I_{ps}^{MZ} = \frac{1}{2}(G + g)^2\alpha_{in}^2 + g^2$. Then the sensitivity of QMZI is

$$\delta_{QMZI} = \sqrt{\frac{1 + (1 - l_1)(1 - l_2)[(G - g)^2 - 1]}{2(1 - l_1)(1 - l_2)(I_{ps}^{MZ} - g^2)}}, \quad (9)$$

Sensitivity of QMZI can be enhanced by a factor of $2G$ in comparison with the SNL ($\sqrt{1/2I_{ps}}$) when the phase-sensing intensity is larger than the square of the gain factor g^2 and $G \gg 1$ in the lossless case. To describe the experimental performance of the quantum interferometer, the signal-to-noise ratio improvement (SNRI) is given by $SNRI = -20\text{Log}_{10}(\delta/\delta_{SNL})$, which is related to its sensitivity.

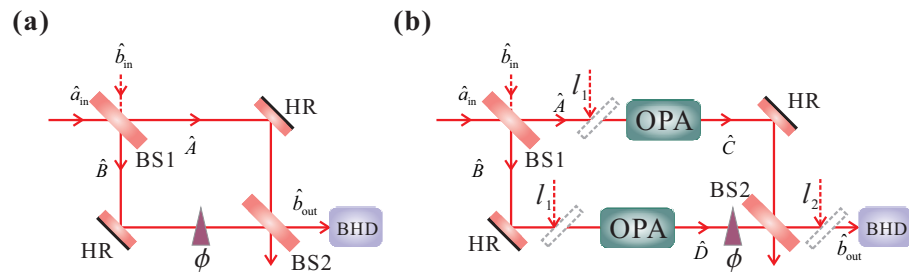


Figure 2. (a,b) Schematic diagrams of linear Mach-Zehnder interferometer and quantum Mach-Zehnder interferometer based on OPAs, respectively. The coherent state \hat{a}_{in} and the vacuum state \hat{b}_{in} are injected into the interferometer, and the phase signal can be obtained by detecting the output optical field \hat{b}_{out} . OPA, optical parametric amplifier; BHD, balanced homodyne detection; BS_{1,2}, 50:50 beam splitter; HR, high-reflection mirror; ϕ , phase shift; l_1 , internal loss of single arm; l_2 , total external loss.

3. Results and Discussion

By comparing and analyzing the relationship between measurement sensitivity and system parameters of the two kinds of quantum interferometers, such as the intensity of optical fields for phase sensing, the gain factor of OPA, and the losses inside and outside the interferometers, the application conditions of high-sensitivity nonlinear quantum interferometers can be obtained. Figure 3 shows the effect of the OPA gain G_p on the sensitivity of the quantum interferometer. As the sensitivity of the interferometer increases with the increase in the intensity of the phase-sensitive light field, in order to more accurately compare the sensitivity, we choose the same phase-sensitive light field intensity $I_{ps} = 1/2G_p\alpha_{in}^2$ as the standard [35]. The input α_{in}^2 of the interferometer is $4.5 \times 10^{13} \text{ s}^{-1}$ (the corresponding input laser power is $10.0 \mu\text{W}$) and 10 s^{-1} in Figure 3a and Figure 3b, respectively. The black trace, red trace, and blue trace correspond to the SNL, δ_{QMI} , and δ_{QMZI} , respectively; the green dashed trace expresses the HL. It can be seen that the sensitivity of both kinds of quantum interferometers can exceed the SNL and be improved with the increase in the OPA gain. When the OPA gain is small ($G_p < 3$), QMI performs better than QMZI. With the further increase in OPA gain, the advantage of QMZI in effectively exploiting shot noise squeezing shows, and the sensitivity is higher. Moreover, the sensitivity of QMZI can approach the HL with the low phase-sensitive light field intensity.

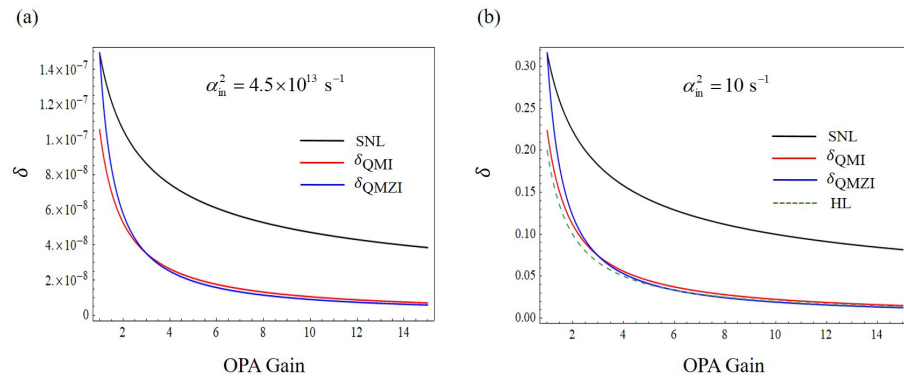


Figure 3. (a,b) Dependence of the sensitivity on OPA gain with the input $\alpha_{in}^2 = 4.5 \times 10^{13} \text{ s}^{-1}$ and $\alpha_{in}^2 = 10 \text{ s}^{-1}$, respectively. The black trace, red trace, blue trace, and green dashed trace correspond to the SNL, δ_{QMI} , δ_{QMZI} , and HL, respectively.

The effect of losses on the sensitivity of the two quantum interferometers is analyzed in detail by calculating the relationship between losses and SNRI. The dependence of SNRIs of the two quantum interferometers on internal loss l_1 and total external loss l_2 is shown in Figure 4a,b. The OPA gain is 15 and the input α_{in}^2 of interferometer is $4.5 \times 10^{13} \text{ s}^{-1}$. The sensitivity of the two quantum interferometers decreases with the increase in internal and external losses, and the measurement sensitivity can be significantly improved by reducing the loss of the system. Specially, the SNRI of QMZI is extremely sensitive to both kinds of loss, and decreases sharply as the losses increases. Meanwhile the SNRI of QMI is only sensitive to internal loss; the external loss has little influence on its sensitivity. Therefore, QMI is more suitable for the case of high external loss.

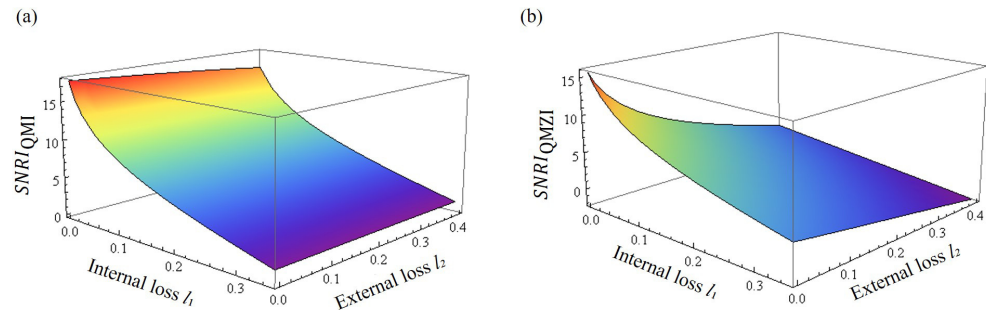


Figure 4. (a,b): Dependence of SNRIs of QMI and QMZI on internal loss l_1 and total external loss l_2 , respectively.

The sensitivities of quantum interferometers versus the phase-sensing intensity of the phase-sensing fields are illustrated in Figure 5. The dash traces and solid traces correspond to the realistic situation ($l_1 = 0.005, l_2 = 0.15$) and the lossless case, respectively. The black trace, red traces, and blue traces correspond to the SNL, δ_{QMI} , and δ_{QMZI} when the OPA gain is 15, respectively. When the input α_{in}^2 of the interferometer is $4.5 \times 10^{13} \text{ s}^{-1}$, the corresponding value of δ_{SNL} is 3.8×10^{-8} [15]. The calculated value of δ_{QMI} and δ_{QMZI} can be improved to 7.0×10^{-9} and 6.3×10^{-9} in the lossless case, which is a 5.5-fold and 6.1-fold enhancement beyond the above SNL.

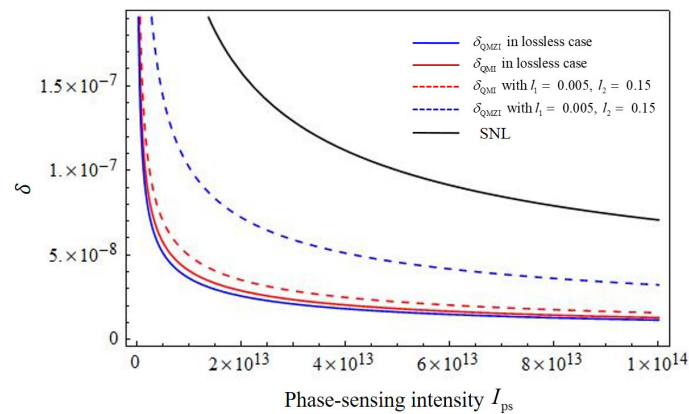


Figure 5. Dependence of the sensitivities on phase-sensing intensity when the OPA gain is 15. The dash traces and solid traces correspond to realistic situation ($l_1 = 0.005, l_2 = 0.15$) and the lossless case, respectively. The black trace, red traces, and blue traces correspond to the SNL, δ_{QMI} , and δ_{QMZI} , respectively.

4. Conclusions

Through analyzing in detail the influence of system parameters on the precision of quantum metrology, the application conditions of high-sensitivity nonlinear quantum interferometers are obtained. The two quantum interferometers not only squeeze shot noise, but also amplify the phase-sensing intensity to realize the sensitivity beyond the SNL. When the OPA gain is small ($G_P < 3$), QMI performs better than QMZI. With the further increase in OPA gain, the advantage of QMZI in effectively exploiting shot noise squeezing shows; the sensitivity is higher, and the sensitivity of QMZI can approach the HL with low phase-sensitive light field intensity. The SNRI of QMI is only sensitive to the internal loss of the interferometer; the external loss has little influence on its sensitivity when the OPA gain is 15. Meanwhile, QMI is more suitable for the case of the high external loss of the interferometer. Our result provides a direct reference of the experimental implementation of high-performance interferometers for high-precision quantum metrology.

Author Contributions: Conceptualization, J.Y. and X.Z.; methodology, J.Y.; software, J.Y.; validation, Y.W., L.N. and X.Z.; formal analysis, J.Y.; investigation, J.Y. and X.Z.; resources, J.Y.; data curation, Y.W.; writing—original draft preparation, J.Y.; writing—review and editing, J.Y.; visualization, J.Y.; supervision, L.N.; project administration, J.Y.; funding acquisition, J.Y., Y.W. and X.Z. All authors have read and agreed to the published version of the manuscript.

Funding: This research was funded by the National Natural Science Foundation of China (Grant Nos. 62105256, 12103039), Young Talent fund of University Association for Science and Technology in Shaanxi, China (Grant No. 20230103), Scientific Research Program Funded by Shaanxi Provincial Education Department, China (Grant No. 21JK0694), the Natural Science Basic Research Program in Shaanxi Province of China (Grant No. 2021JQ-640), and the Social Development Science and Technology Project of Dongguan City (Grant No. 20231800903222).

Institutional Review Board Statement: Not applicable.

Informed Consent Statement: Not applicable.

Data Availability Statement: The data presented in this study are available on request from the corresponding author.

Conflicts of Interest: The authors declare no conflict of interest.

References

1. Taylor, M.A.; Janousek, J.; Daria, V.; Knittel, J.; Hage, B.; Bachor, H.-A.; Bowen, W.P. Sub diffraction-Limited Quantum Imaging within a Living Cell. *Phys. Rev. X* **2014**, *4*, 011017.
2. Giovannetti, V.; Lloyd, S.; Maccone, L. Advances in quantum metrology. *Nat. Photonics* **2011**, *5*, 222–229. [[CrossRef](#)]

3. Tse, M.; Yu, H.; Kijbunchoo, N.; Fernandez-Galiana, A.; Dupej, P.; Barsotti, L.; Blair, C.D.; Brown, D.D.; Dwyer, S.E.; Effler, A.; et al. Quantum-Enhanced Advanced LIGO Detectors in the Era of Gravitational-Wave Astronomy. *Phys. Rev. Lett.* **2019**, *123*, 231107. [[CrossRef](#)]
4. Acernese, F.; Agathos, M.; Aiello, L.; Allocca, A.; Amato, A.; Ansoldi, S.; Antier, S.; Arene, M.; Arnaud, N.; Ascenzi, S.; et al. Increasing the Astrophysical Reach of the Advanced Virgo Detector via the Application of Squeezed Vacuum States of Light. *Phys. Rev. Lett.* **2019**, *123*, 231108. [[CrossRef](#)]
5. Kimble, H.J.; Levin, Y.; Matsko, A.B.; Thorne, K.S.; Vyatchanin, S.P. Conversion of conventional gravitational-wave interferometers into quantum nondemolition interferometers by modifying their input and/or output optics. *Phys. Rev. D* **2001**, *65*, 022002. [[CrossRef](#)]
6. Peters, A.; Chung, K.Y.; Chu, S. High-precision gravity measurements using atom interferometry. *Metrologia* **2001**, *38*, 25. [[CrossRef](#)]
7. Rosi, G.; Sorrentino, F.; Cacciapuoti, L.; Prevedelli, M.; Tino, G. Precision measurement of the Newtonian gravitational constant using cold atoms. *Nature* **2014**, *510*, 518–521. [[CrossRef](#)] [[PubMed](#)]
8. Gault, W.; Shepherd, G. WAMDII—A wide angle Michelson Doppler imaging interferometer for spacelab. *Adv. Space Res.* **1982**, *2*, 111–114. [[CrossRef](#)]
9. Boixo, S.; Davis, M.J.; Shaji, A. Quantum Metrology: Dynamics versus Entanglement. *Phys. Rev. Lett.* **2008**, *101*, 040403. [[CrossRef](#)]
10. Holland, M.J.; Burnett, K. Interferometric detection of optical phase shifts at the Heisenberg limit. *Phys. Rev. Lett.* **1993**, *71*, 1355. [[CrossRef](#)]
11. Xiao, M.; Wu, L.A.; Kimble, H.J. Precision Measurement beyond the Shot-Noise Limit. *Phys. Rev. Lett.* **1987**, *59*, 278. [[CrossRef](#)]
12. Grangier, P.; Slusher, R.E.; Yurke, B.; LaPorta, A. Squeezed-Light-Enhanced Polarization Interferometer. *Phys. Rev. Lett.* **1987**, *59*, 19. [[CrossRef](#)]
13. Degen, C.L.; Reinhard, F.; Cappellaro, P. Quantum sensing. *Rev. Mod. Phys.* **2017**, *89*, 035002. [[CrossRef](#)]
14. Ma, Y.; Miao, H.; Pang, B.H.; Evans, M.; Zhao, C.; Harms, J.; Schnabel, R.; Chen, Y. Proposal for gravitational-wave detection beyond the standard quantum limit through EPR entanglement. *Nat. Photonics* **2017**, *13*, 776–780. [[CrossRef](#)]
15. Ou, Z.Y. Enhancement of the phase-measurement sensitivity beyond the standard quantum limit by a nonlinear interferometer. *Phys. Rev. A* **2012**, *85*, 023815. [[CrossRef](#)]
16. Caves, C.M. Quantum mechanical noise in an interferometer. *Phys. Rev. D* **1981**, *23*, 1693. [[CrossRef](#)]
17. Huang, Z.X.; Motes, K.R.; Anisimov, P.M.; Dowling, J.P.; Berry, D.W. Adaptive phase estimation with two-mode squeezed vacuum and parity measurement. *Phys. Rev. A* **2017**, *95*, 053837. [[CrossRef](#)]
18. Liu, F.; Zhou, Y.Y.; Yu, J.; Guo, J.L.; Wu, Y.; Xiao, S.X.; Wei, D.; Zhang, Y.; Jia, X.J.; Xiao, M. Squeezing-enhanced fiber Mach-Zehnder interferometer for low-frequency phase measurement. *Appl. Phys. Lett.* **2017**, *110*, 021106. [[CrossRef](#)]
19. Higgins, B.L.; Berry, D.W.; Bartlett, S.D.; Wiseman, H.M.; Pryde, G.J. Entanglement-free Heisenberg-limited phase estimation. *Nature* **2007**, *450*, 393–396. [[CrossRef](#)] [[PubMed](#)]
20. Xiang, G.Y.; Higgins, B.L.; Berry, D.W.; Wiseman, H.M.; Pryde, G.J. Entanglement-enhanced measurement of a completely unknown optical phase. *Nat. Photonics* **2010**, *5*, 43–47. [[CrossRef](#)]
21. Yonezawa, H.; Nakane, D.; Wheatley, T.A.; Iwasawa, K.; Takeda, S.; Arao, H.; Ohki, K.; Tsumura, K.; Berry, D.W.; Ralph, T.C.; et al. Quantum-enhanced optical phase tracking. *Science* **2012**, *337*, 1514–1517. [[CrossRef](#)]
22. Yu, J.; Qin, Y.; Qin, J.L.; Wang, H.; Yan, Z.H.; Jia, X.J.; Peng, K.C. Quantum Enhanced Optical Phase Estimation With a Squeezed Thermal State. *Phys. Rev. Appl.* **2020**, *13*, 024037. [[CrossRef](#)]
23. Guo, X.S.; Breum, C.R.; Borregaard, J.; Izumi, S.; Larsen, M.V.; Gehring, T.; Christandl, M.; Neergaard-Nielsen, J.S.; Andersen, U.L. Distributed quantum sensing in a continuous variable entangled network. *Nat. Phys.* **2020**, *16*, 281–284. [[CrossRef](#)]
24. Dinani, H.T.; Berry, D.W. Adaptive estimation of a time-varying phase with a power-law spectrum via continuous squeezed states. *Phys. Rev. A* **2017**, *95*, 063821. [[CrossRef](#)]
25. Nagata, T.; Okamoto, R.; O'Brien, J.L.; Sasaki, K.; Takeuchi, S. Beating the Standard Quantum Limit with Four-Entangled Photons. *Science* **2007**, *316*, 726–729. [[CrossRef](#)]
26. Huo, M.R.; Qin, J.L.; Cheng, J.L.; Yan, Z.H.; Qin, Z.Z.; Su, X.L.; Jia, X.J.; Xie, C.D.; Peng, K.C. Deterministic quantum teleportation through fiber channels. *Sci. Adv.* **2018**, *4*, eaas9401. [[CrossRef](#)]
27. Zhou, Y.Y.; Yu, J.; Yan, Z.H.; Jia, X.J.; Zhang, J.; Xie, C.D.; Peng, K.C. Quantum Secret Sharing among Four Players Using Multipartite Bound Entanglement of an Optical Field. *Phys. Rev. Lett.* **2018**, *121*, 150502. [[CrossRef](#)] [[PubMed](#)]
28. Yan, Z.H.; Qin, J.; Qin, Z.Z.; Su, X.L.; Jia, X.J.; Xie, C.D.; Peng, K.C. Generation of non-classical states of light and their application in deterministic quantum teleportation. *Fundam. Res.* **2021**, *1*, 43–49. [[CrossRef](#)]
29. Ma, L.X.; Lei, X.; Yan, J.L.; Li, R.Y.; Chai, T.; Yan, Z.H.; Jia, X.J.; Xie, C.D.; Peng, K.C. High-performance cavity-enhanced quantum memory with warm atomic cell. *Nat. Commun.* **2022**, *13*, 2368. [[CrossRef](#)] [[PubMed](#)]
30. Nichols, R.; Bromley, T.R.; Correa, L.A.; Adesso, G. Practical quantum metrology in noisy environments. *Phys. Rev. A* **2016**, *94*, 042101. [[CrossRef](#)]
31. Yurke, B.; McCall, S.L.; Klauder, J.R. SU(2) and SU(1,1) interferometers. *Phys. Rev. A* **1986**, *33*, 4033. [[CrossRef](#)] [[PubMed](#)]
32. Hudelist, F.; Kong, J.; Liu, C.; Jing, J.; Ou, Z.Y.; Zhang, W. Quantum metrology with parametric amplifier-based photon correlation interferometers. *Nat. Commun.* **2014**, *5*, 3049. [[CrossRef](#)]

33. Zheng, K.M.; Mi, M.H.; Wang, B.; Xu, L.Y.; Hu, L.; Liu, S.S.; Lou, Y.B.; Jing, J.T.; Zhang, L.J. Quantum-enhanced stochastic phase estimation with SU(1,1) interferometer. *Photonics Res.* **2020**, *8*, 1653–1661. [[CrossRef](#)]
34. Li, J.M.; Liu, Y.H.; Cui, L.; Huo, N.; Assad, S.M.; Li, X.Y.; Ou, Z.Y. Joint measurement of multiple noncommuting parameters. *Phys. Rev. A* **2018**, *97*, 052127. [[CrossRef](#)]
35. Zuo, X.J.; Yan, Z.H.; Feng, Y.N.; Ma, J.X.; Jia, X.J.; Xie, C.D.; Peng, K.C. Quantum interferometer combining squeezing and parametric amplification. *Phys. Rev. Lett.* **2020**, *124*, 173602. [[CrossRef](#)]
36. Pooser, R.C.; Savino, N.; Batson, E.; Beckey, J.L.; Garcia, J.; Lawrie, B.J. Truncated nonlinear interferometry for quantum-enhanced atomic force microscopy. *Phys. Rev. Lett.* **2020**, *124*, 230504. [[CrossRef](#)] [[PubMed](#)]
37. Huang, W.; Liang, X.; Zhu, B.; Yan, Y.; Yuan, C.; Zhang, W.; Chen, L.Q. Protection of Noise Squeezing in a Quantum Interferometer with Optimal Resource Allocation. *Phys. Rev. Lett.* **2023**, *130*, 073601. [[CrossRef](#)] [[PubMed](#)]
38. Heinze, J.; Danzmann, K.; Willke, B.; Vahlbruch, H. 10 dB Quantum-Enhanced Michelson Interferometer with Balanced Homodyne Detection. *Phys. Rev. Lett.* **2022**, *129*, 031101. [[CrossRef](#)]
39. Zander, J.; Rembe, C.; Schnabel, R. 10 dB interferometer enhancement by squeezing of photon shot noise with sub-femtometer resolution and eye-safe optical power. *Quantum Sci. Technol.* **2023**, *8*, 01LT01. [[CrossRef](#)]
40. Kalinin, N.; Dirmeier, T.; Sorokin, A.A.; Anashkina, E.A.; Sánchez-Soto, L.L. Quantum-enhanced interferometer using Kerr squeezing. *Nanophotonics* **2023**, 00323. [[CrossRef](#)]
41. Zuo, X.; Sun, Y.; Yan, Z.; Jia, X. High sensitivity quantum Michelson interferometer. *Acta Phys. Sin.* **2018**, *67*, 134202.

Disclaimer/Publisher's Note: The statements, opinions and data contained in all publications are solely those of the individual author(s) and contributor(s) and not of MDPI and/or the editor(s). MDPI and/or the editor(s) disclaim responsibility for any injury to people or property resulting from any ideas, methods, instructions or products referred to in the content.